LA-UR-21-23854
Approved for public release; distribution is unlimited.

Title: Shocked Transport: Experiments to Study Dynamic Particle Behavior under Varying Volume Fraction Conditions

Author(s): Hughes, Kyle Thomas
Charonko, John James

Intended for: pRad Proposal

Issued: 2021-04-20

Shocked Transport: Experiments to Study Dynamic Particle Behavior under Varying Volume Fraction Conditions

Principle Investigators:

Kyle Hughes[1]

John Charonko

[1]Mailstop H803, Los Alamos National Laboratory, Los Alamos, NM, 87545. Phone: 505-667-6983, Email: kylethughes89@lanl.gov

Motivation

Shocks interacting with densely-packed porous media is common in volcanic eruptions or in engineering applications such as ordinance. Large-scale, exploratory experiments have been performed by Frost and collaborators[1–4] examining the behavior of a bed of particles subjected to a detonation wave. The detonation replaces the central explosive with a high-density, high-temperature gas that propagates outward. A shock wave travels through the particle bed, followed by a contact discontinuity between the shocked air and the explosive products. In the early times, the detonation wave causes many of the particles to collide and compact with each other. As the particles disperse, the experiments demonstrate a series of large-scale jets or fingers that form in the advancing particle front.

Small scale experiments by Sun, Tanno, and collaborators[5–7] have measured the forces on a single, stationary particle subjected to a moderate shock. When comparing the experimental results to drag relations proposed as compressible generalizations of the Maxey-Riley-Gatignol equation[8,9], the generalized force formula captures the magnitude and the timing of the peak force quite well [10–12]. Shock-tube experiments examining the behavior of moving particles have been performed by variety of researchers [13–16]. In these experiments, the position of the particle is observed after being subjected to a shock and the time-varying drag force extracted. Together these small scale experiments provide a wealth of validation data in the modest Mach number regime for a single particle for the proposed drag force relations. Hughes et al. [17] attempted to extend the validation data for a single particle, where the particles are subjected both to a high Mach number shock and a strong contact discontinuity.

Similar to the investigations of a single particle, other investigations have been performed where many particles are subjected to a moderate Mach number shock. In this regime, not only are the individual drag forces important, but the particles compact and collide with each other as well. Figure 1 provides an illustration demonstrating the rich physics present. However, the flows still lack the strong shock and contact discontinuity present in detonation conditions. Dilute suspensions of particles ($\varphi < 1\%$) subjected to a shock have been studied extensively by researchers such as Rudinger [18]. Less common is examination of multiphase flows where moderate to large volume fractions are present ($\varphi > 5\%$). Wagner et al. [19] examined shock wave impingement on a free-falling particle curtain of approximately 20% volume fraction by tracking the upstream and downstream particle fronts through high-speed Schlieren photography. Wagner also provided X-ray photography to measure the volume fraction as it evolved downstream of the shock but was limited to a single exposure per test. Under very similar experimental conditions, Kellenberger at al. [20] examined the behavior of stationary particle wafers of approximately 48% volume fraction subjected to a shock wave through high-speed photography. Note in these studies the volume fraction is less than the 60% commonly found in particle beds typical for the explosive dispersal of particles [21].

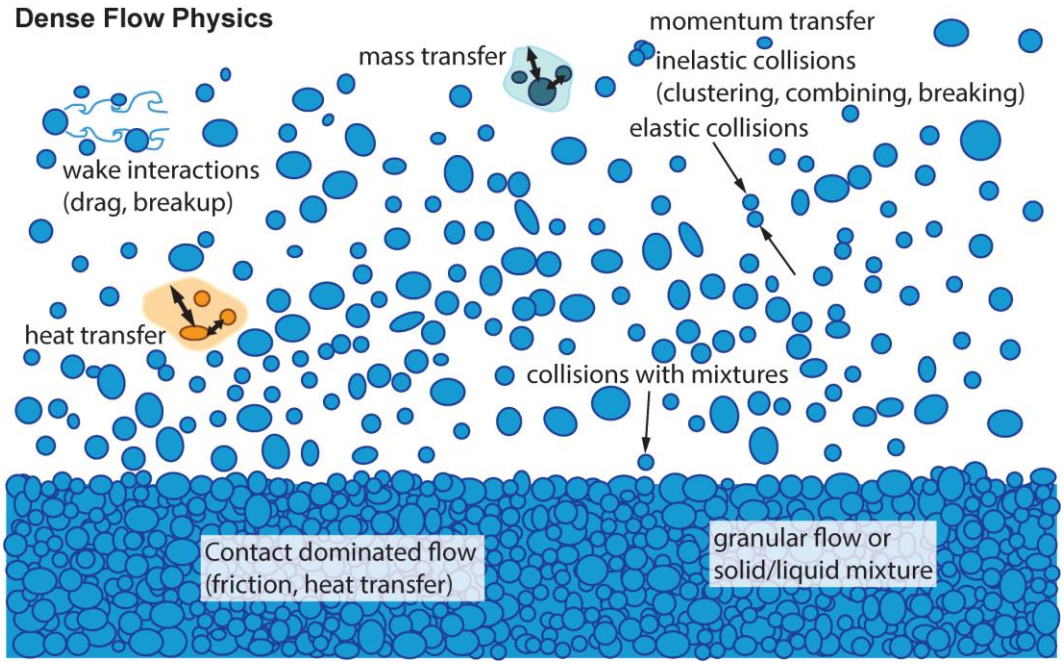

Figure 1: Conceptual sketch of the rich physics present in the high volume fraction regime.

Examining the experiments available in the literature, understanding the dynamics of particle transport during high volume fraction conditions subjected to a high Mach number cases is still very much an open question. The goal with these experiments is to provide validation data to modelers within this regime at the laboratory scale.

Physics Goals & Experimental Concept

Science Campaign 1 is interested in understanding the dynamics of particle transport during high volume fraction conditions, especially in the re-shock of ejecta. In prior work done for the CCMT PSAAPII center, the focus was on understanding particle bed breakup under tension, but breakup structures could not be fully identified due to the optical diagnostics in use and the complex geometry of the experiments. The goal of the proposed experiments is to simplify the particle bed and drive conditions to understand breakup and also drag under dynamic, unsteady load conditions (shock drive) and as a function of volume fraction. This experiment is complementary to ongoing studies at the horizontal shock tube facility, where experiments are examining low volume fraction conditions and looking at individual particle motion.

The proposed experiments are aimed at providing a testbed for new high volume fraction models of ejecta and were designed in conjunction with personal from P, T, and XCP. Figure 2 provides a conceptual sketch of the proposed experiments. In these tests, a plane wave lens will be used to deliver an almost flat shock to a loosely bound bed of particles. Proton radiography will allow examination of the internal structure of the bed not possible with high-speed video. In addition, a series of experiments testing the effect of variation in volume fraction will also be examined. Several simplifying conditions may be implemented at the small scale not possible with large-scale experiments. First, the experiment will be designed with a planar, 1D geometry to simplify the flow, similar to a shock-tube experiment. Second, a planar lens will be used to subject the particles to a high-velocity shock (~2000 m/s) while an

aluminum bulkhead will be used to block the explosive gases, removing the complication of a contact interface. Third, xenon will be used as the ambient fluid to maintain an ideal equation of state even at the high Mach numbers present (Ma_s~12.5). The use of xenon gas and a 1D, planar geometry will allow use of the normal shock relation to recover the post-shock flow. Knowledge of the post-shock flow will allow non-dimensionalization, an improvement over past explosive dispersal experiments.

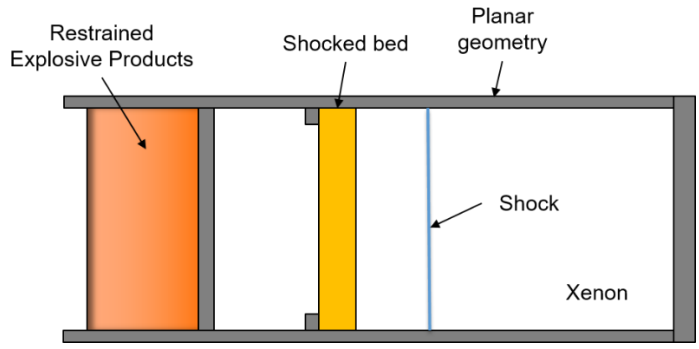

Figure 2: Conceptual sketch of the proposed experiments.

Previous Proton Radiography Investigations

The new experiments will be a significant departure from two previous sets of proton radiography (pRad) experiments conducted by this investigator. Those experiments were intended to provide validation data for CMT-nek, a multiphase code developed at the Center for Compressible Multiphase Turbulence (CCMT) at the University of Florida. The previous two sets of experiments were catered to meeting the simulation capability of CMT-nek. As CMT-nek was a fluid mechanics solver only, it lacked the capability of including solid mechanics such as a deforming casing. Large emphasis was placed in the experimental design on having rigid boundary conditions such that no fragmentation and minimum deformation was observed by using thick steel casings to constrain the explosive products and the particles. In addition, computational resources were somewhat limited and the number of particles used was kept to a relatively small number in an attempt to make the problem more tractable.

More importantly, CCMT was concerned with studying the explosive dispersal of particles. In the explosive dispersal of particles a central explosive is used to disperse an annular dry bed of particles. In this problem, the contact discontinuity between the explosive products and the surrounding fluid is a driving mechanism of the particle dispersal. In the previous experiments, the explosive products were allowed to pass over the particle bed in order to include these important physics. Here, the explosive products will be constrained to focus more carefully on the shock interaction with the particle beds.

However, the two previous sets of experiments have given insight that is still relevant to the current proposed experiments and so will be summarized here. The two sets of previous experiments will be referred to by their time of testing: October 2017 (Oct17) and November 2018 (Nov18). Each set of experiments performed 5 explosive shots. Each shot recorded 21 radiographs spaced 2 µs apart with a resolution of 844x853 pixels. The x3 magnifier was used to provide a 45-mm by 45-mm field of view with a resolution of 50 µm/pixel. Tests were performed within the 6’ vessel.

Details of the test article, used in both the Oct17 and Nov18 test series, are shown in Figure 3. A 10.2-cm outer diameter steel casing (AISI 4340) was used with a central bore of 13.1-mm nominal diameter and a

depth of 19.1 mm. The casing showed minor deformation post-test, but no fragmentation was observed. Examination of post-detonation photographs shows the bore diameter increased from 13.1 mm to 15±3 mm, an increase of approximately 15%. A pellet of PBX-9501 (12.7 mm diameter with 12.7 mm length) was initiated by a Teledyne RISI RP-80 exploding bridgewire detonator. Time was measured from detonator initiation, determined from a current viewing resister, with approximately ±0.1 µs uncertainty.

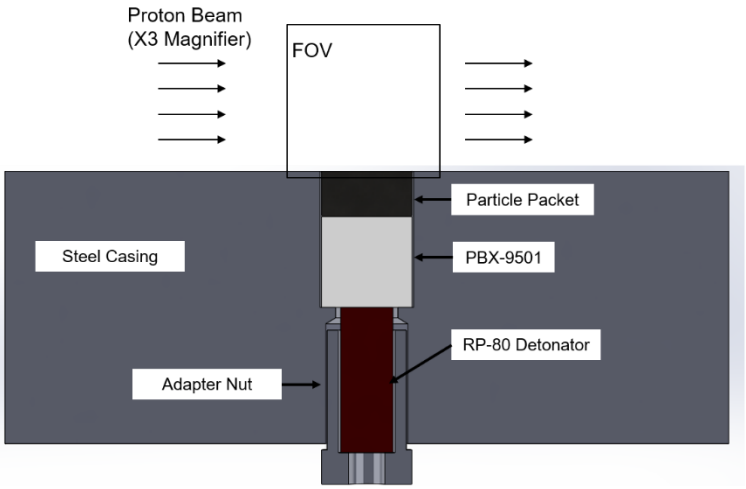

Figure 3: Details of the test article used in Oct17 and Nov18 test series. An RP-80 detonator was used initiate a pellet of PBX-9501 explosive. The explosive then dispersed a 13.1 mm by 6.35 mm bed of particles.

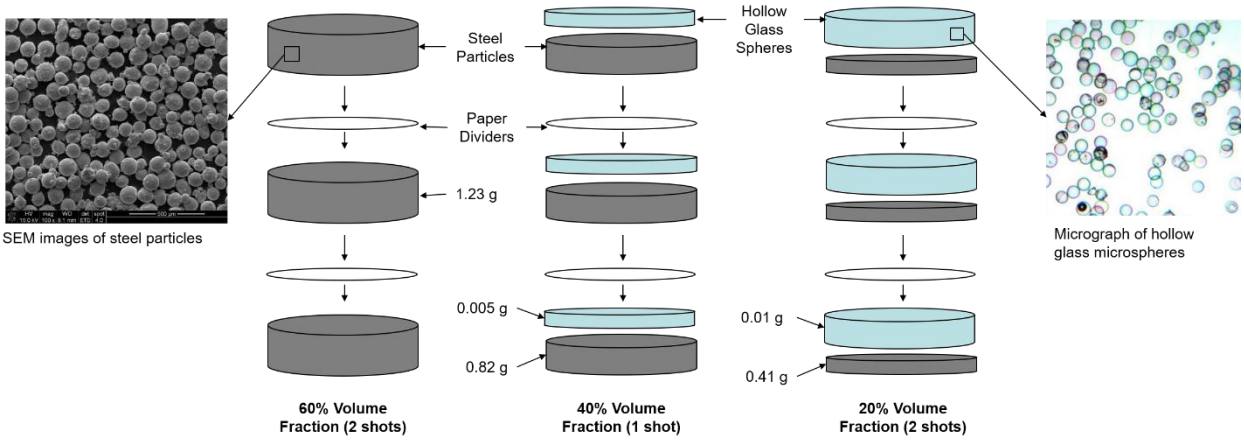

Figure 4: Details of the three configurations used for the particle packet. Accompanying high-magnification images of the particles used are included. (Hollow glass microsphere micrograph credit: Cospheric).

For the Oct17 test series, the tests were performed within the vacuum provided by the 6' vessel. In addition, for the Oct17 tests, the particle packet volume fraction was reduced with the use of hollow glass microspheres (HGM). Figure 4 shows details of the particle packet assembly. Three configurations were investigated: 60%, 40%, and 20% total volume fraction. Three layers were used for each particle packet with paper dividers separating the layers. Steel particles (410 alloy, sieved 75-125 µm, obtained from Sandvik Osprey) were used as a base. The HGM were sieved 90-125 µm and obtained from Cospheric. The test articles were oriented vertically so the particles were held in place by gravity before

detonation. A piece of tape was placed over the particle bed to prevent spillage of the bed during loading. The particles were packed to approximately 56±1% volume fraction and no binder was used to constrain their movement.

Transmission radiographs of the five explosive tests at 20 μs after detonation initiation are shown in Figure 5. The 60% volume configuration shows a "piston-like behavior" as it is expelled by the explosive. The three initial layers maintain their structure as they are expelled from the barrel and exhibit minimal spreading. At late times, some slow intermixing of the layers is exhibited. The 40% volume fraction configuration has the three-layer structure initially visible as it exits the casing but quickly devolves into a cloud as it travels downstream. The 20% volume fraction case exits as a cloud with single denser line present and shows a greater stochastic nature. The overall shape may be observed to be largely different in curvature between the repeated tests for the 20% case. Note for the 60% case, that portions of the bed seem to exhibit cracks. However, these cracks do not seem to be visible with the lower volume fraction shots.

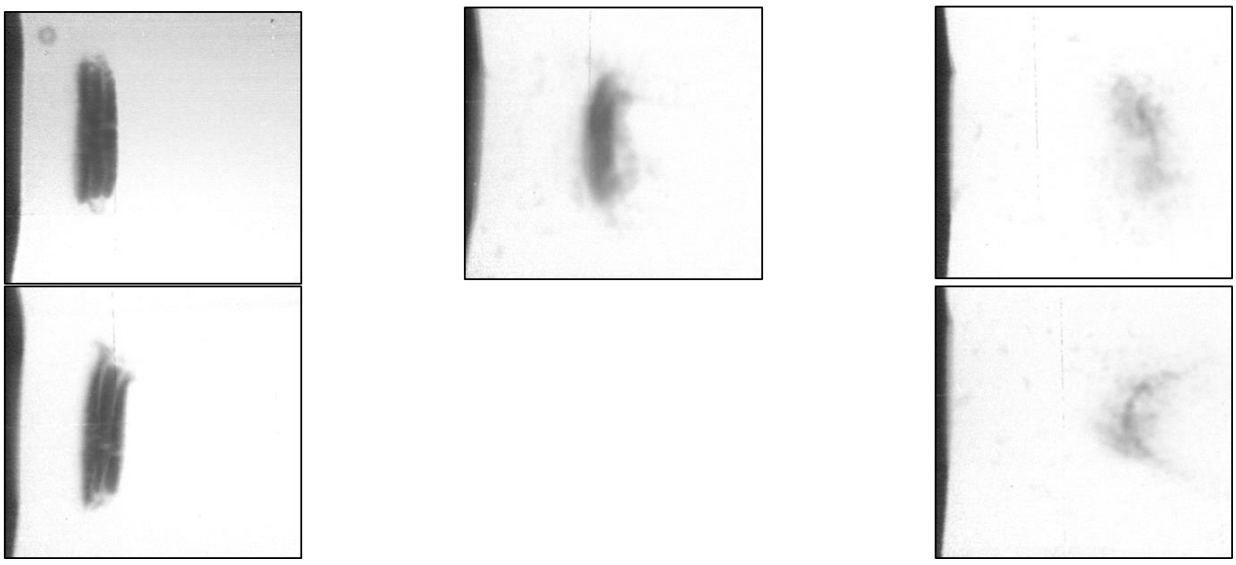

a) b) c)

Figure 5: Oct17 transmission radiographs 20 μs after detonation for: a) 60% volume fraction, b) 40% volume fraction, and c) 20% volume fraction. Multiple images for a given volume fraction represent repeated tests. Flow is from left to right.

For the Nov18 test series, the particle packet was made of only steel particles (nominally the same as the 60% case in the Oct17 case). The steel particles were the same as those used in the Oct17 test and were again divided into three layers of 1.233±0.001 g by paper dividers (3.697±0.002 g total). No binder was used in this test as well, though tape was still necessary to maintain the bed during loading. However, the Nov18 test series introduced an ambient fluid to the setup by wrapping the test article with a 6.35-mm thick aluminum cylinder. Three carrier phases were investigated: air, xenon, and SF_6. A baseline vacuum test was also performed. A gas handling system was used to ensure each cylinder was brought to approximately 100 kPa pressure and the temperature recorded to determine the initial thermodynamic state of the gas. The temperature was measured to be 298.4 ± 0.9 K and the measured pressure was 100.6 ± 0.8 kPa.

Sample transmission radiographs of the four different test conditions 40 µs after detonation initiation are shown in Figure 6. Note that an aluminum ring was placed around the lip of the steel casing to secure it and is visible in the radiographs as a thin layer of less dense material above the dark steel casing. Two screws used to secure the aluminum ring are also visible at the edges of the radiographs. The particle packet shows again piston-like behavior as it is expelled by the explosive. The three initial layers maintain their structure as they are expelled from the barrel and exhibit minimal spreading. At late times, some slow intermixing of the layers is exhibited. Though small differences in structure and spreading are apparent, the particles are remarkably close to each other considering the varying initial conditions.

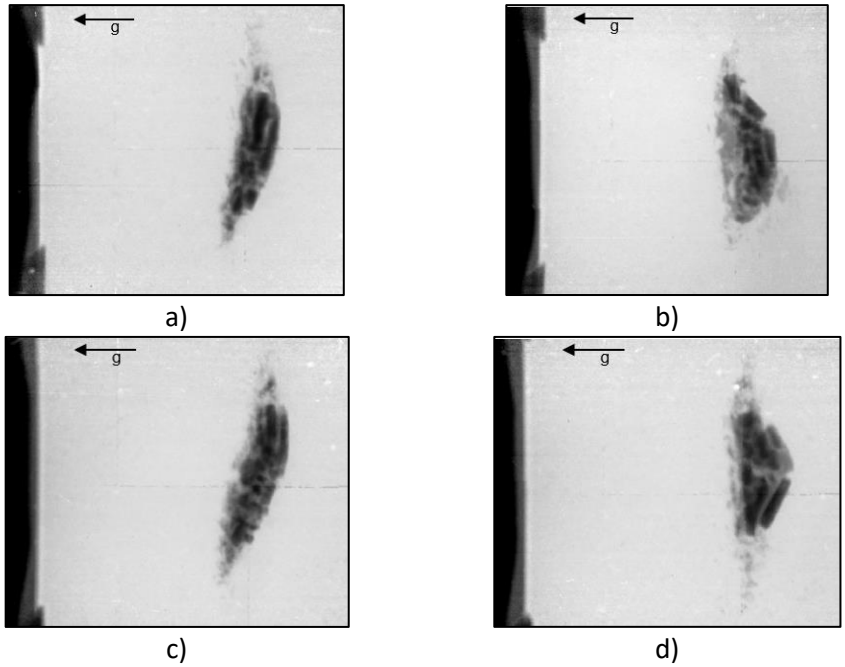

Figure 6: Nov18 transmission radiographs showing the dispersal of the particles 40 µs after detonator initiation for the four different test configurations: a) air, b) xenon, c) SF6, d) vacuum. Flow is from left to right.

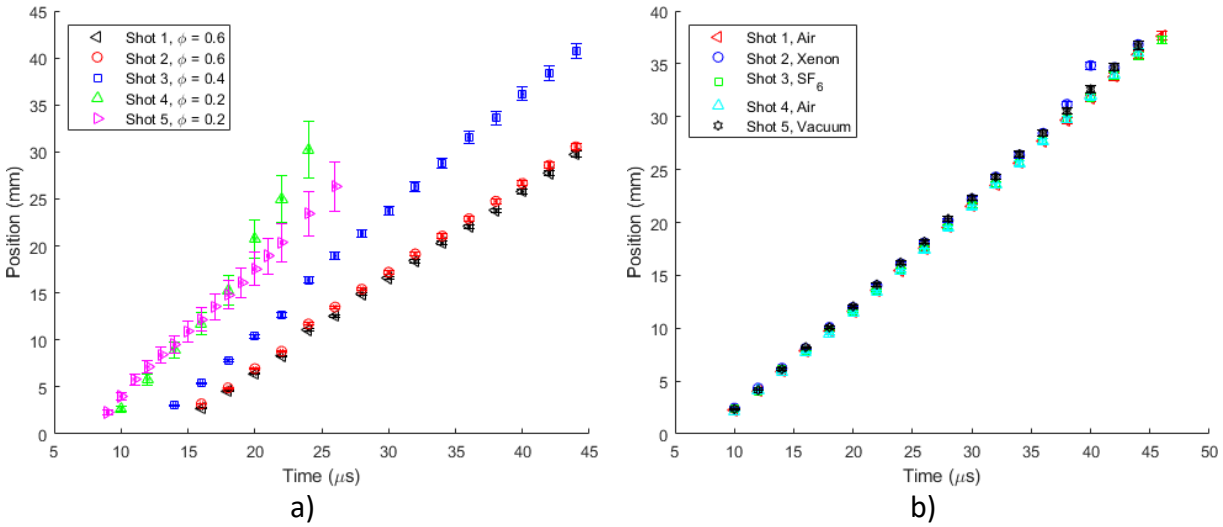

Figure 7: Centerline downstream particle fronts obtained from the radiographs. a) Oct17. b) Nov18.

The downstream particle front (corresponding to the top of the particle bed) are determined from thresholding of the transmission intensity. The downstream particle front from both test series at the centerline was extracted and plotted in Figure 7. The initial time in the plots is detonator initiation. An approximately 4 μs delay is present for the detonator to activate and for the explosive to completely react. For the Oct17 front positions, the repeated tests show close agreement on the centerline except for the upstream front position 20% case. One may observe an increase in overall packet velocity as the total mass of the particle bed is decreased with the addition of hollow glass microspheres. The 20% volume fraction quickly exited the field of view for the 2 μs interframe time and so relatively few data points were recovered in Shot 4. For the Nov18 tests, the fonts were remarkably similar to one another given the large differences in density and speed of sound from one medium to the other. The centerline results demonstrate a highly linear behavior during this early time suggesting that the particles are impulsively acted upon by the contact interface and the shock. Furthermore, comparing the results of the four gas shots with the vacuum shot, we note that the results are within close agreement. The vacuum shot lacks an ambient medium for a shock to form, suggesting that the contact interface between the ambient fluid and the HE products is almost solely responsible for the delivered impulse. Results for these experiments have been published in Shock Waves[22].

Lessons Learned

From the previous pRad experiments, several key insights can be gained that guide the proposed series of experiments:

1) While the thick, rigid casing was advantageous for the simulation validation, it prevents interrogation of the particle bed during the initial compaction phase where important early time behaviors (particle compaction, collisions, etc.) are occurring.
2) Definite curvature is noted in the dispersed particle packet, suggesting the shock and/or explosive front is not yet flattened for the simple explosive train used.
3) The shock (present for ambient fluid shots) is not observed even with higher Z-number gases such as xenon. An improved test article design may improve the results but additional diagnostics such as piezo-electric pins should be used to allow recovery of the shock.
4) The 3D geometry and complex equation of state prevent non-dimensionalization of the flow for comparison to laboratory studies. Delaying the explosive products and use of a 1D geometry would allow use of normal shock relations to recover the post-shock flow.
5) The loose beds may have been perturbed during the loading process based on some of irregularities observed. The thick casing prevented observation of the bed before the arrival of the detonation wave to confirm or deny this possibility.

Proposed Experiment: Shocked Transport

Proton Radiography Configuration

The proposed experiment will use the 6’ diameter explosive chamber for the proton radiography test section. To examine the fine detail of the bed during dispersal, the x3 magnifier lens is proposed. A proof shot is scheduled to be performed by J-division to assess the need for blast mitigation. The proof-shot will also be used to confirm timings and the working of the secondary diagnostics. The confirmatory is scheduled to be performed the week of 1/25/2021.

Test Article

A schematic of the proposed shot is presented in Figure 8. As can be seen in the radiographs of the previous pRad experiments presented, the dispersed particle packets displayed a curved front, even in the case of vacuum shots. To correct this, extra care is being taken in the proposed experiments to subject the particle bed to a flat shock by replacing the previous RP-80 detonator and PBX-9501 pellet with a P-25 plane wave lens initiated by a RP-1 detonator. CTH simulations provided by Anna Llobet of the P-25 lens have been provided in Figure 9. The CTH simulations show the arriving shock front is close to flat, with less than 20 ns difference in time of arrival from the center to 4 mm. Further data, not shown, shows there is approximately 200 ns difference in time of arrival from the center to the edge of the P-25 lens. Further pre-shot calculations are currently being performed in FLAG to refine shot timings but are not yet completed.

The aluminum casing surrounding the high explosive is similar to that used by Anna Llobet and collaborators. The 2 mm thick aluminum bulkhead will be used to delay the explosive products from interacting with the particle bed. As shown in previous pRad experiments, if the explosive products are allowed to interact with the particles the contact discontinuity would dominate the drag of the particles and prevent study of the shock interaction. In addition, the delay of the explosive products allows a much simplified equation of state. The chosen thickness has been demonstrated experimentally by Anna Llobet not to spall.

A 3D printed bed of steel particles, printed by Lawrence Bronisz on an ExOne printer, will be placed 40 mm downstream of the 2-mm thick aluminum. The steel particles (440 alloy) are sized 13-60 μm and pack to approximately 55.7% volume fraction (see the Uncertainty Quantification section for further details). The method used to lower the volume fraction will be detailed in the next section. Four phase Doppler velocimetry (PDV) probes will be used to redundantly measure the surface velocity of the steel particles and check for asymmetry of the particle motion. A tungsten fiducial is included to allow extraction of the areal density of the particle bed in the case of beam fluctuation. Note that a small notch, not shown, was placed on one side of the particle bed to allow the xenon to flow around the particle bed and completely fill the canister.

The ambient fluid is chosen to be xenon, for its large radiographic cross section. Xenon, as a monotonic gas, also allows the use of an ideal equation of state even to very high Mach numbers. The xenon will be pumped to a pressure of 200 kPa to further increase the chance of recovering the shock radiographically. The initial pressure and temperature will be measured to determine the thermodynamic state of the carrier phase. As a further technique for measuring the shock speed, pressure transducers are installed along the side of the tube.

Once impulsively put into motion, the particles are allowed to propagate along a narrow tube. The narrow tube was chosen to restrict the flow to be almost 1D and increase the radiographic quality. The advantage of the 1D geometry, along with the simple equation of state, allows calculation of the post-shock fluid velocity through normal shock relations. If shock relations may be used and post-shock conditions known, the results may be non-dimensionalized, an advantage over previous pRad experiments.

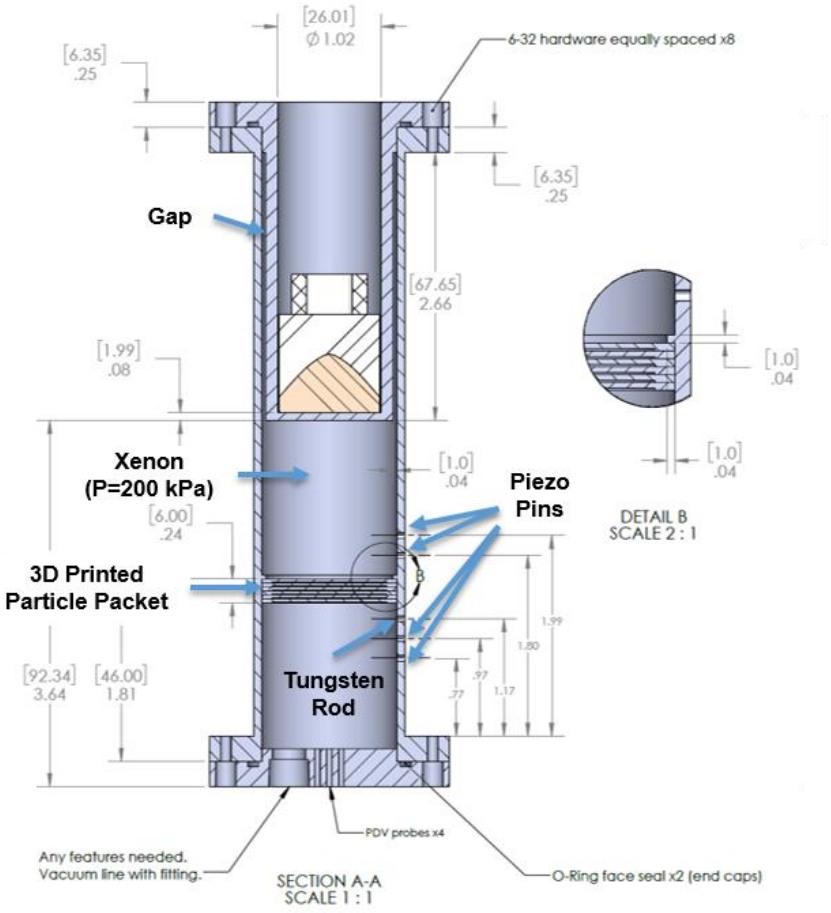

Figure 8: Proposed test article. Bracketed dimensions are in millimeters and are otherwise in inches. The particle packet is dispersed by a P-25 lens, initiated by a RP-1 detonator. A thin 2-mm layer of aluminum is used to delay the explosive products from interacting with the particle bed. Piezo-electric pins are used to measure the shock time of arrival upstream and downstream of the particle packet. Xenon is used as a carrier fluid to allow use of an ideal equation of state and radiographing of the shock. The initial thermodynamic state of the xenon is recorded with temperature and pressure probes teed off the input gas line. The PDV probes are used to measure the surface velocity of the particle bed. A tungsten fiducial is used to extract the areal density.

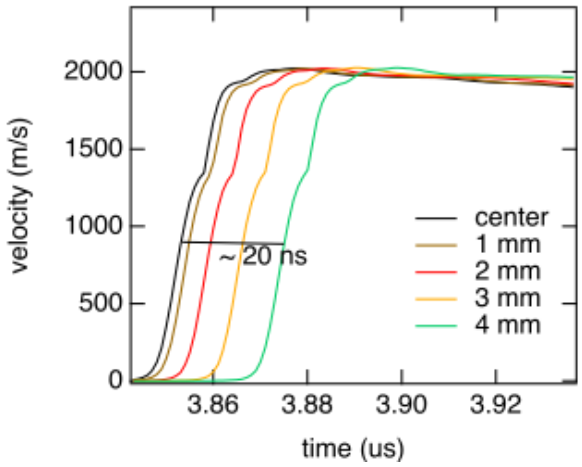

Figure 9: Velocity profiles of the P-25 lens, obtained from simulation in CTH and provided by Anna Llobet. The velocity profiles show a surface velocity of 2000 m/s at the end of the P-25 lens. In addition, there is less than 20 ns difference in time of arrival from the center to 4 mm.

Shot Configuration

Five total explosive shots are proposed, shown in Table 1. The particle beds are nominally 33 mm in diameter and 6 mm in depth. 3D printing of the particle beds allows the introduction of fine layers. By leaving the printed parts in their uncured state, the particle beds are extremely fragile, breaking without careful handling. In their uncured state, the steel particles pack to approximately 56%. To lower the volume fraction, the particle packet is sub-divided into six layers. Hemispherical dimples are then introduced to the front and back of the layers in an approximately hexagonal close packing arrangement to remove material and lower the global volume fraction of the layer. By keeping the dimples as small as possible, the local volume fraction begins to approximate the global volume fraction. However, the dimples must be of sufficient size to allow the removal of loose, unbound powder as well leaving enough material to provide structural integrity to the remaining layer so it does not disintegrate during assembly. The resulting dimple diameter was 1 mm with the smallest wall thickness between two dimples reduced to 180 µm. The lowest global volume fraction that could be achieved with these restraints was 32%.

Table 1: Volume fraction configuration for the five proposed shots.

Shot	φ	Layers	Layer Thickness (mm)	Collimator (mrad)
1	0.56	1	6	7.5
2	0.56	6	1	7.5
3	0.42	6	1	7.5
4	0.32	6	1	7.5
5	0.32	6	1	5

Models of the three volume fractions are shown in Figure 10. Due to the fragility of the lower volume fraction layers, a solid ring of 1 mm was left on the outside portion of the layer to provide some additional strength. In addition, two versions of the layer were constructed so that the dimples would

form spherical voids when matched together. A clocking mechanism, in the form of a protrusion, was placed on the outside ring.

Measurement of the shock is critical to success of the experiments. The piezo-pins provide this critical information but are un-tested in this configuration. To first establish their efficacy and agreement with the radiographs, the 5 mrad collimator will be used on the lowest volume fraction case. The smaller amount of steel particles provides sufficient contrast to still provide some sense of physics occurring within the bed, though not optimal, while still measuring the gas shock. However, once sufficient confidence has been between the piezo-pins and radiograph, the minimum volume fraction case of 0.32 will be repeated with the 7.5 mrad collimator and used for the rest of the tests. The 7.5 mrad collimator should provide optimal contrast within the bed, though at the cost of directly measuring the gas shock. In addition, to determine the effect of the layers and epoxy used to bond them, one of the 60% cases will consist of a single 6 mm layer while the other will consist of six, 1-mm layers.

The three volume fractions have already been successfully printed and assembled within the test article.

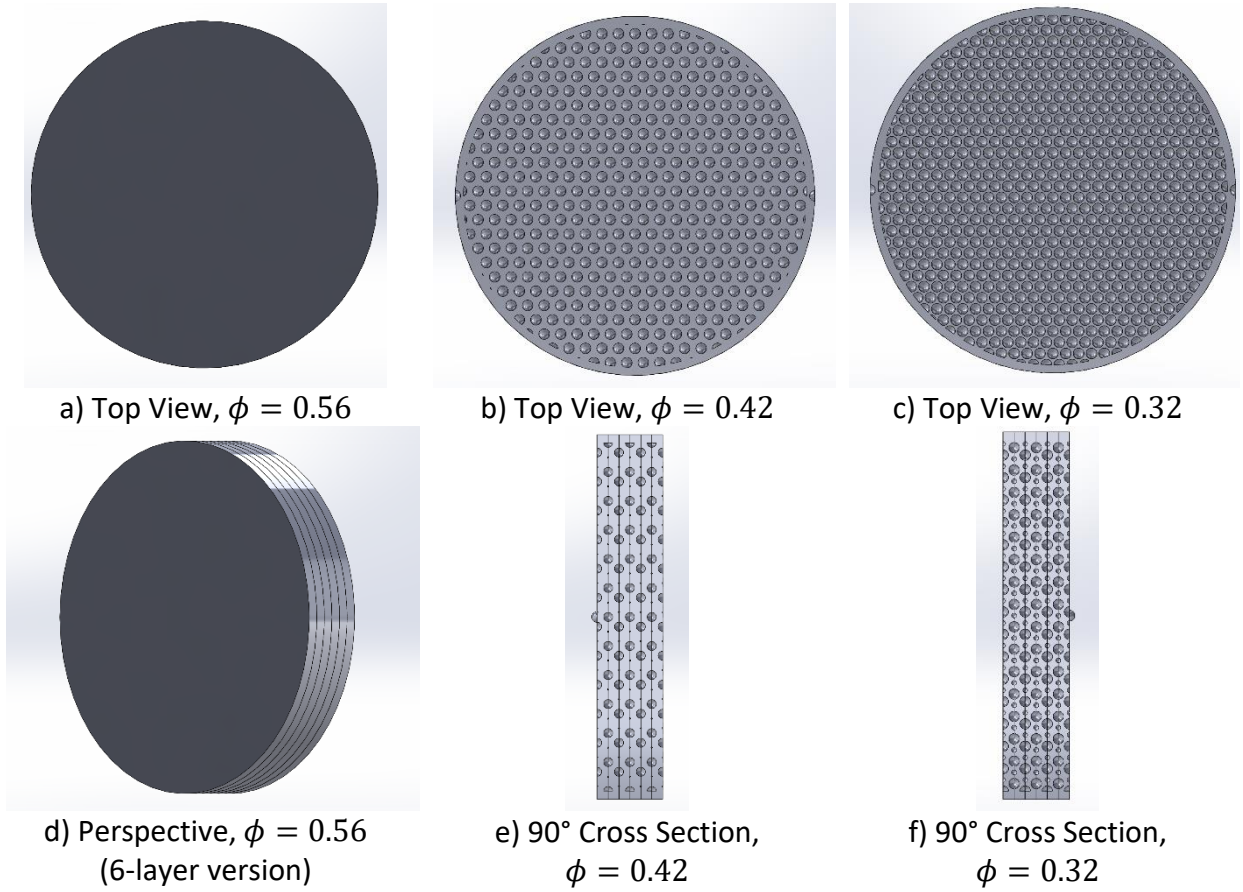

Figure 10: Top views of 3D-printed particle layers of the a) 56%, b) 42%, and c) 32% volume fractions. d) A perspective view of the 6 stacked layers with no material removed. Cross-sectional views of the e) 42% and f) 32% stacked layers showing the spherical voids when two layers are stacked on one another.

Uncertainty Quantification

Uncertainty quantification of the 3D printer has been investigated previously by Lawrence Bronisz and collaborators. Their investigations have shown achievable feature sizes of 64 µm in the x-y direction and 100 µm in the z-direction, similar to tolerances achievable through milling. Furthermore, because the parts are to be left in the green state (un-cured), shrinking of the part during the curing process is not a major concern. Computer tomography (CT) of the 3D printed parts shows an approximately 0.557 volume fraction of the packed particles. Sizing of the particles, also from the CT scan, show particles range in size from approximately 13-60 µm with a mean of 25 µm. In addition, pre-shot statics should sufficiently characterize the bed before arrival of the shock to well characterize the particle bed.

Budget

The cost of the proposed test articles will be covered by the Extreme Fluids group. The particle beds may be 3D-printed at low cost. An itemized list of cost estimates is included in Table 2.

Table 2: Itemized list of estimated costs. The PDV probe cost is neglected as the Extreme Fluids group has a stock of PDV probes already.

Item	Cost ($)
RP-1 Detonators	1,500
P-25 Plane Wave Lenses	12,000
Aluminum stock	600
Pressure Transducers	2,000
Phase Doppler Velocimetry Probes	-
Xenon gas	1,500
3D Printed Particle Beds	500
Machining	25,000
Total	**25,450**

References

1. Zhang, F., Frost, D. L., Thibault, P. a. & Murray, S. B. Explosive dispersal of solid particles. *Shock Waves* **10**, 431–443 (2001).

2. Frost, D. L., Zarei, Z. & Zhang, F. Instability of Combustion Products Interface from Detonation of Heterogeneous Explosives. in *20th International Colloquium on the Dynamics of Explosions and Reactive Systems* 1–6 (2005).

3. Frost, D. L., Ornthanalai, C., Zarei, Z., Tanguay, V. & Zhang, F. Particle momentum effects from the detonation of heterogeneous explosives. *J. Appl. Phys.* **101**, 113529 (2007).

4. Frost, D. L., Grégoire, Y., Petel, O., Goroshin, S. & Zhang, F. Particle jet formation during explosive dispersal of solid particles. *Phys. Fluids* **24**, 091109 (2012).

5. Sun, M., Saito, T., Takayama, K. & Tanno, H. Unsteady drag on a sphere by shock wave loading. *Shock Waves* **14**, 3–9 (2005).

6. Tanno, H., Itoh, K., Saito, T., Abe, A. & Takayama, K. Interaction of a shock with a sphere suspended in a vertical shock tube. *Shock Waves* **13**, 191–200 (2003).

7. Bredin, M. S. & Skews, B. W. Drag Measurement in Unsteady Compressible Flow Part 1: An Unsteady Flow Facility and Stress Wave Drag Balance. *R&D J. South African Inst. Mech. Eng.* **23**, 1–10 (2007).

8. Maxey, M. R. & Riley, J. J. Equation of motion for a small rigid sphere in a nonuniform flow. *Phys. Fluids* **26**, 883–889 (1983).

9. Gatignol, R. The Faxén formulas for a rigid particle in an unsteady non-uniform Stokes-flow. *J. Mécanique théorique appliquée* **2**, 143–160 (1983).

10. Parmar, M., Haselbacher, A. & Balachandar, S. Generalized Basset-Boussinesq-Oseen Equation for Unsteady Forces on a Sphere in a Compressible Flow. *Phys. Rev. Lett.* **106**, 084501 (2011).

11. Parmar, M., Haselbacher, A. & Balachandar, S. Equation of motion for a sphere in non-uniform compressible flows. *J. Fluid Mech.* **699**, 352–375 (2012).

12. Annamalai, S. & Balachandar, S. Faxén form of time-domain force on a sphere in unsteady spatially varying viscous compressible flows. *J. Fluid Mech.* **816**, 381–411 (2017).

13. Britan, A., Elperin, T., Igra, O. & Jiang, J. P. Acceleration of a sphere behind planar shock waves. *Exp. Fluids* **20**, 84–90 (1995).

14. Jourdan, G. *et al.* Drag coefficient of a sphere in a non-stationary flow: new results. *Proc. R. Soc. A Math. Phys. Eng. Sci.* **463**, 3323–3345 (2007).

15. Wagner, J. L., Beresh, S. J., Kearney, S. P., Pruett, B. O. M. & Wright, E. K. Shock tube investigation of quasi-steady drag in shock-particle interactions. *Phys. Fluids* **24**, 123301 (2012).

16. Bordoloi, A. D., Martinez, A. A. & Prestridge, K. Relaxation drag history of shock accelerated microparticles. *J. Fluid Mech.* **823**, R4 (2017).

17. Hughes, K. *et al.* Uncertainty Quantification of Experiments on a Small Number of Explosively-Driven Particles. in *55th AIAA Aerospace Sciences Meeting* 1–14 (American Institute of Aeronautics and Astronautics, 2017). doi:10.2514/6.2017-1463

18. Rudinger, G. Some properties of shock relaxation in gas flows carrying small particles. *Phys. fluids* **658**, 658–663 (1964).

19. Wagner, J. L. *et al.* A multiphase shock tube for shock wave interactions with dense particle fields. *Exp. Fluids* **52**, 1507–1517 (2012).

20. Kellenberger, M., Johansen, C., Ciccarelli, G. & Zhang, F. Dense particle cloud dispersion by a shock wave. *Shock Waves* **23**, 415–430 (2013).

21. Dullien, F. A. L. *Porous Media: Fluid Transport and Pore Structure*. (Elsevier Science, 1992). doi:10.1016/C2009-0-26184-8

22. Hughes, K. T. *et al.* Proton radiography of explosively dispersed metal particles with varying volume fraction and varying carrier phase. *Shock Waves* **123**, 223–230 (2021).